HAL
open science

Development of Nafion/Tin Oxide Composite MEA for DMFC applications

Fang Chen, Barbara Mecheri, Alessandra d'Epifanio, Enrico Traversa, Silvia Licoccia

To cite this version:

Fang Chen, Barbara Mecheri, Alessandra d'Epifanio, Enrico Traversa, Silvia Licoccia. Development of Nafion/Tin Oxide Composite MEA for DMFC applications. Fuel Cells, 2010, 10 (5), pp.790. 10.1002/fuce.200900179 . hal-00578451

HAL Id: hal-00578451

https://hal.science/hal-00578451v1

Submitted on 21 Mar 2011

HAL is a multi-disciplinary open access archive for the deposit and dissemination of scientific research documents, whether they are published or not. The documents may come from teaching and research institutions in France or abroad, or from public or private research centers.

L'archive ouverte pluridisciplinaire **HAL**, est destinée au dépôt et à la diffusion de documents scientifiques de niveau recherche, publiés ou non, émanant des établissements d'enseignement et de recherche français ou étrangers, des laboratoires publics ou privés.

Fuel Cells

Development of Nafion/Tin Oxide Composite MEA for DMFC applications

Journal:	*Fuel Cells*
Manuscript ID:	fuce.200900179.R2
Wiley - Manuscript type:	Original Research Paper
Date Submitted by the Author:	19-Apr-2010
Complete List of Authors:	Chen, Fang; University of Rome Tor Vergata, Department of Chemical Science and Technology Mecheri, Barbara; University of Rome Tor Vergata, Department of Chemical Science and Technology D'Epifanio, Alessandra; University of Rome, Chemical Science and Technology Traversa, Enrico; International Center for Materials Nanoarchitectonics (MANA), National Institute for Materials Science (NIMS); University of Rome Tor Vergata, Department of Chemical Science and Technology Licoccia, Silvia; University of Rome Tor Vergata, Department of Chemical Science and Technology
Keywords:	Direct Methanol Fuel Cell, Proton Exchange Membrane, Nafion, Methanol Crossover, Performance Improvement

scholarONE™
Manuscript Central

Development of Nafion/Tin Oxide Composite MEA for DMFC applications

F.Chen[1], B.Mecheri[1], A.D'Epifanio[1], E.Traversa[1,2], and S.Licoccia[1*]

[1] Department of Chemical Science and Technology, University of Rome "Tor Vergata", Via della Ricerca Scientifica, 00133 Rome, Italy
[2] International Center for Materials Nanoarchitectonics (MANA), National Institute for Materials Science (NIMS), 1-1 Namiki, Tsukuba, Ibaraki 305-0044, Japan

Received

[*] Corresponding author, licoccia@uniroma2.it

Abstract

Nafion composite membranes containing either hydrated tin oxide ($SnO_2 \cdot nH_2O$) or sulfated tin oxide (S-SnO_2) at 5 wt.% and 10 wt.% were prepared and characterized. The structural and electrochemical features of the samples were investigated using X-ray diffraction, electrochemical impedance spectroscopy, methanol crossover, and direct methanol fuel cell (DMFC) tests. Highest conductivity values were obtained by using S-SnO_2 as filler (0.094 Scm^{-1} at T=110°C and RH=100%). The presence of the inorganic compound resulted in lower methanol crossover and improved DMFC performance with respect to a reference unfilled membrane. To improve the interface of the membrane electrode assembly (MEA), a layer of the composite electrolyte (*i.e.*, the Nafion membrane containing 5 wt% S-SnO_2) was brushed on the electrodes, obtaining a DMFC operating at 110°C with a power density (PD) of 100 $mWcm^{-2}$ which corresponds to a PD improvement of 52% with respect to the unfilled Nafion membrane.

Keywords: Direct Methanol Fuel Cells, Proton Exchange Membrane, Nafion, Methanol Crossover, Performance Improvement.

1 Introduction

Extensive research in the fields of materials chemistry and engineering has been carried out over the last decades with the aim of improving the efficiency of Direct Methanol Fuel Cells (DMFC) [1-4].

In particular, much work has been directed towards understanding the structure and proton transport properties of Nafion, the most widely used electrolyte for DMFC applications [5-7]. Despite its high proton conductivity and excellent chemical stability, Nafion performance, especially at high temperatures, is impaired by methanol crossover through the polymer membrane and by conductivity decay above 90 °C [8]. These drawbacks have been associated with the anisotropic swelling that Nafion undergoes at high temperature which damages the membrane dimensional stability [9] and also gives rise to interfacial complications, including high resistance and poor adhesion between membrane and electrodes [10].

Improved performance, both in terms of higher operating temperature and lower methanol crossover, have been reported for a variety of composite membranes [11-13]. In the case of composites containing hygroscopic oxides, such as SiO_2, TiO_2, or ZrO_2, as fillers, the results have been attributed to the effect of filler surface characteristics on the water retention properties of the composite and/or to morphological variations of the composite membrane with respect to unfilled Nafion [14-16]. The amount of filler must be carefully controlled since an excessive loading of a non conducting inorganic species may be detrimental for the overall proton conductivity of the composite Nafion membrane [17].

To minimize proton conductivity losses induced by the incorporation of inorganics, the use of proton conducting fillers has been explored.

In particular, zirconium phosphate/Nafion composites have been found to exhibit a stable conductivity behavior up to 140 °C at RH = 90% [18,19]. The enlarged stability domain of proton conductivity has been related to the higher stiffness of the composite membranes and thus to their enhanced dimensional stability [20]. The use of acidic fillers, such as heteropolyacids or sulfated metal oxides, has been also explored [21-25]. The acidic surface functionalities of inorganic fillers have been found to play a key role towards the improvement of the water retention properties of the composite membrane and thus of their transport properties. By an appropriate tailoring of the surface characteristics

For Peer Review

of different fillers (such as SiO_2, PWA-SiO_2, ZrO_2, Al_2O_3), the power density of Nafion-based DMFCs have been improved up to 0.4 Wcm^{-2} [26].

To obtain electrolytes characterized by good proton transport features, reduced methanol crossover and enhanced dimensional stability at T > 90 °C, in this work we selected hydrated tin oxide ($SnO_2 \cdot nH_2O$) and its sulfated derivative (S-SnO_2) as fillers for the Nafion matrix.

$SnO_2 \cdot nH_2O$ is an inorganic proton conductor; when used as filler in a sulfonated polyether ether ketone (SPEEK) matrix gives rise to composites characterized by higher proton conductivity and lower methanol crossover than those of an unfilled SPEEK due to its capability to selectively reduce the tortuosity of the SPEEK membrane for proton transport and to avoid methanol permeation through the membrane [27,28]. Among all known solids, sulfated tin oxide (S-SnO_2) is currently recognized as one of the strongest superacids [29, 30].While largely used as catalyst [31,32], to our knowledge S–SnO_2 has never been explored as filler in composite polymer electrolyte membranes. With the aim of providing additional acidic sites to enhance proton transport, we exploited S–SnO_2 as filler of the Nafion membrane.

We here report a comparison of the properties of Nafion-based composites obtained by using either $SnO_2 \cdot nH_2O$ or S–SnO_2 and analyze the influence of the oxide surface acidic functionalization.

2 Experimental

2.1 Materials

2.1.1 Preparation of $SnO_2.nH_2O$ and S-SnO_2

Hydrated tin oxide ($SnO_2 \cdot nH_2O$) was prepared according to the procedure previously reported [27, 28]. Sulfated tin oxide (S-SnO_2) was obtained as follows [29]: $SnO_2 \cdot nH_2O$ was suspended in 3 M sulfuric acid and stirred for 1 h at room temperature, then filtered and dried at room temperature for 1 h. Finally, the powder was calcined at 500 °C in air for 3 h and then milled in an agate mortar.

2.1.2 Preparation of composite membranes

Composite membranes at 5 wt.% and 10 wt.% filler content were prepared as follows. Nafion perfluorinated resin solution at 5 wt.% in a mixture of lower aliphatic alcohols and water (Sigma–Adrich, CAS number 31175-20-9) (12 mL) was added to dimethylacetamide (DMA). The solution was heated to 80 °C to evaporate low-boiling solvents. During the evaporation step DMA was added to maintain the solution volume around 15 mL. This process was repeated three times to ensure that the original solvent was replaced by DMA. 5 and 10 wt% (with respect to Nafion content) of either $SnO_2 \cdot nH_2O$ or S-SnO_2 was dispersed in DMA and the resulting suspension was treated in an ultrasonic bath for 4 hours and then added to the Nafion solution. The suspension was then casted in a petri dish and dried at 80 °C overnight. Unfilled Nafion membranes were also prepared and used as reference. The thickness of the membranes ranged between 90-120 µm. Before characterization, all the membranes were treated in a standard activation procedure using H_2O_2 3 vol % solution, 0.5 M H_2SO_4 solution and distilled water, boiling the samples for 1hour in each solution.

2.2 Methods

2.2.1 XRD, EDX, FT-IR, and TG analyses

The X-ray diffraction (XRD) analysis was carried out at room temperature by a PW 1729 X-ray generator (Philips International, Inc.) equipped with a CuKα radiation source and graphite monochromator. XRD patterns were collected in the 2θ range of 5°-60° (step size: 2 θ = 0.02°; time per step: 2 s).

The energy dispersive X-ray (EDX) microanalysis was performed at 10 keV using an INCA Energy 300 spectrometer.

Fourier-transformed infrared spectra (FT-IR) were acquired by means of a Nexus 670 Thermo Nicolet FT-IR spectrometer (128 scans at a resolution of 4 cm^{-1}). The powders were pelleted with KBr and analyzed in transmission mode. The ion exchange capacity (IEC) of the oxide powders was measured by potentiometric titrations [33]. A typical amount of 20 mg of sample was dried at 60 °C under vacuum for 2 hours and then immersed in a 0.1 M NaCl overnight to exchange protons to Na^+ ions. The resulting solution were titrated with a 0.1 M NaOH solution to neutralize exchanged proton.

Thermogravimetric analysis (TG) was carried out in the 25–1000 °C temperature range, using a thermobalance (STA 409, Netzsch), in air flow (80 $mLmin^{-1}$) with a heating rate of 2 °C $min^{-1}s$).

2.2.2 Conductivity

Through-plane conductivity measurements were carried out on membrane disks of 6 mm in diameter, sandwiched between gas diffusion electrodes (E-Tek ELAT HT 140E-W with a Pt loading of 5 mg cm^{-2}).

For Peer Review

By means of a Multichannel Potentiostat VMP3 (Princeton Applied Research), impedance spectra were acquired, applying a voltage of 20 mV in a frequency range of 10 Hz – 1 MHz. The membrane conductivity was calculated according to the equation 1:

$$\sigma = d/RA \qquad \text{(Eq.1)}$$

where R is the membrane resistance, d the distance between electrodes and A is the electrode area. Conductivity of membranes was measured at 100°C and 110°C at 100% relative humidity.

2.2.3 DMFC performance, in situ EIS, and methanol permeation measurements.

Commercial Hydro2Power electrodes were used as anode and cathode, respectively: A-6 ELAT/SS/PtRu60-3-30PTFE/0.8N, custom 3 $mgcm^{-2}$ loading using 60% HP Pt:Ru alloy (1:1) on Vulcan, 30 wt% PTFE with 0.8 $mgcm^{-2}$ Nafion , and A-6 ELAT/SS/Pt40-2-30PTFE/0.8N custom 2 $mgcm^{-2}$ loading using 40% HP Pt on Vulcan, 30 wt% PTFE with 0.8 $mgcm^{-2}$ Nafion. The membrane electrode assembly (MEA) was prepared, as extensively described in a previous work [34] sandwiching electrolyte membranes between anode and cathode by hot pressing at 120 °C under 3.75 MPa for 7 minutes.

A brushing technique was used to prepare functionalized electrodes. The commercial anode and cathode were treated in a vacuum oven at 80 °C for 2 hours and then they were brushed with a 5 wt.% S-SnO_2/Nafion suspension in DMA. The brushed electrodes were placed in the vacuum oven at 80 °C for 2 hours to eliminate DMA residues and they were assembled with N_5S-SnO_2 membrane to prepare MEA.

DMFC performance was evaluated by placing the MEA in a single cell (ElectroChem) with active area of 5 cm^2. A homemade test station was used, feeding the anode with a 2 M methanol solution and the cathode with humidified oxygen. The feeding supply of methanol was monitored by a KNF's Model FEM 1.08 Liquid Metering Pump with control board (flow rate: 2.5 $mLmin^{-1}$, pressure: 2 abs bar). The oxygen supply was controlled by a MKS PR4000 mass-flow controller (flow rate: 100 sccm, pressure: 2 abs bar), and the humidifier temperature was opportunely set to ensure 100% RH of the gas [34]. Polarization and power density curves were obtained using a Multichannel Potentiostat VMP3 (Princeton Applied Research) in the temperature range between 70 and 110 °C.

In situ EIS measurements were performed during the cell functioning, in potentiostatic mode (0.3 V). An AC sinusoidal perturbation (amplitude 15 mV) was introduced to the DC load, and impedance spectra were acquired by sweeping frequencies over the 500 kHz – 1 Hz range recording 10 points per decade.

For methanol permeation measurements, linear sweep voltammetry (LSV) was used to measure the steady-state limiting current density at cathode due to the oxidation of methanol permeating from the anode side. During the course of the experiment, the anode was fed by 2 M methanol solution at a flow rate of 2 $mLmin^{-1}$. Humidified N_2 was fed into the cathode. The limiting current density (J_{lim}) was measured at 80 °C, applying a voltage from 0 to 0.85 V (scan rate: 2 mVs^{-1}).

3 Results and Discussion

Figure 1 shows the XRD patterns of hydrated tin oxide ($SnO_2 \cdot nH_2O$), and sulfated tin oxide (S-SnO_2) powders. The XRD pattern of $SnO_2 \cdot nH_2O$ is characterized by broad peaks which reveal an amorphous-like state of the oxide. Some sharpening of the peaks, without any detectable shift, was observed in the XRD pattern of S-SnO_2 as a result of increased crystallinity induced by heating to 500 °C.

The energy dispersive x-ray (EDX) microanalysis was used to assess and quantify the sulfur presence on the surface of the tin oxide particles. Figure 2 compares the EDX spectra of $SnO_2 \cdot nH_2O$ (Fig. 2a) and S-SnO_2 (Fig. 2b). While the EDX spectrum of $SnO_2 \cdot nH_2O$ displayed only the peaks due to tin and oxygen, the spectrum of S-SnO_2 showed a further peak due to the sulfur presence. The Sn:O:S atomic ratio in the sulfated sample resulted to be 66.1:32.1:1.8.

In order to elucidate the structural features of the sulfur functionalities, FT-IR spectra were acquired on both oxides. Figure 3 shows the FT-IR spectra of $SnO_2 \cdot nH_2O$ and S-SnO_2. The $SnO_2 \cdot nH_2O$ sample displayed a broad absorption band in the region 3600-2500 cm^{-1} which can be ascribed to H-bonded hydroxyl groups coupled with physisorbed water molecules. The band centered at 1600 cm^{-1} corresponds to -OH bending mode of water molecules[35, 36]. The FT-IR spectra of the sulfated samples shows some differences both in the frequency region of O-H stretching and, especially, in the frequency range of the SO_4^{2-} stretching vibration. In particular, the shoulder at 2870 cm^{-1} associated to the main peak became more evident, this being ascribed to hydroxyls perturbations induced by neighboring sulfate groups. Moreover, new absorption bands at 975, 1050, 1152, 1213 cm^{-1} are clearly visible. According to previous literature reports [37-39], the main peak centered at 1150 cm^{-1} can be ascribed to the symmetric stretching of S=O vibrations, the splitting of this peak being characteristic of the formation of bidentate sulfate groups coordinated to the tin particles.

For Peer Review

To evaluate the effect of the functionalization on the surface acidity of the tin oxide, IEC values of both oxide powders were measured and they were found to be 0.352 meq g^{-1} and 1.42 meq g^{-1}, for $SnO_2 \cdot nH_2O$ and S-SnO_2, respectively. These values are in good agreement with ion-exchange capacity of metal oxides including hydrated tin oxide [40-42]. The increased IEC of the sulfated sample revealed the enhanced acidity of S-SnO_2 with respect to $SnO_2 \cdot nH_2O$ provided by the surface functionalization of the filler.

To study the thermal evolution of the two fillers, thermogravimetric (TG) analysis was carried out on the oxide powders. Figure 4 shows the TG curves of $SnO_2 \cdot nH_2O$ and S-SnO_2 powders. As far as $SnO_2 \cdot nH_2O$ is concerned, the main weight loss (about 12 % of the total loss), observed in the 50–150 °C range, can be attributed to the loss of physisorbed water, while the loss of structural and bound water occurred gradually between 250 and 450 °C [43-45]. The TG profile of S-SnO_2 shows two different weight losses; the first one, occurring in the 50–150 °C range, corresponds to water desorption, whereas the weight loss occurring in the 600-760 °C range (about 4% of the total loss) can be attributed to the splitting off of sulfate groups bound to the surface of SnO_2 crystallites [46]. TG analysis thus revealed that the acidic surface functionalities are thermally stable in the temperature range of interest for DMFC applications.

Composite Nafion-based membranes containing 5 wt.% and 10 wt.% of either $SnO_2 \cdot nH_2O$ (N_5SnO_2 and N_10SnO_2) or S-SnO_2 (N_5S-SnO_2 and N_10S-SnO_2) were prepared. To evaluate the suitability of such composites as proton conducting electrolytes, proton conductivity (σ) of all membranes was measured and the corresponding values at 100 °C and 110 °C are shown in Figure 5. At both temperatures, σ of the composites was higher than that of a reference Nafion recast membrane (N_RC) with the exception of N_10SnO_2 where the decrease of proton charge carriers caused by the presence of a large amount of filler appears to dominate the electrochemical properties. The highest σ values were shown by membrane N_5S-SnO_2 as a result of the enhanced acidity of S-SnO_2 with respect to $SnO_2 \cdot nH_2O$ provided by the surface functionalization of the filler [47]. σ values are indeed all comprised in a narrow range, each sample meeting proton conductivity requirements for DMFC applications [48].

It is noteworthy that proton conductivity of the unfilled Nafion membrane decreased as the temperature increased from 100 °C to 110 °C, whereas σ of the 5 wt.% composites increased. It appears then that at such loading the presence of the filler allowed to extend to higher temperatures the stability range of proton conductivity. This finding is in good agreement with previous work on the effect of superacid zirconia on the proton conductivity of Nafion membranes [12,23,25].

To check the applicability of the composite Nafion based membranes in a real device, the electrochemical performance of the membranes was tested in a DMFC single cell, acquiring polarization curves. Figure 6 shows polarization (I-V) and power density (PD) curves for the unfilled Nafion and composite membranes at T=100 °C (Fig. 6a) and T=110 °C (Fig. 6b). At T=100 °C, the unfilled Nafion and the N_5SnO_2 sample showed similar performance (PD_{max} = 68 $mWcm^{-2}$, $I_{(0.15V)}$ = 370 $mAcm^{-2}$, for N_5SnO_2 sample), whereas the performance of N_5S-SnO_2 sample was found to be higher (PD_{max} = 76 $mWcm^{-2}$ and $I_{(0.15V)}$ = 415 $mAcm^{-2}$).

Increasing the temperature from 100 °C to 110 °C caused a decrease of the N_RC membrane performance, according to its well-known loss in stability above 90 °C. On the contrary, the N_5SnO_2 sample maintained almost the same PD and I values with respect to those recorded at 100 °C, whereas the performance of the N_5S-SnO_2 sample kept increasing (PD_{max}= 82 $mWcm^{-2}$ and $I_{(0.15V)}$ = 443 $mAcm^{-2}$). Such enhancement cannot be ascribed exclusively to the difference in conductivity values which were not so dissimilar to justify the improved PD and I curves.

To better understand the reasons why composites showed a performance superior to that of the unfilled Nafion membrane, firstly we evaluated the effect of the filler on methanol crossover. Limiting methanol permeation current density (J_{lim}) values through the unfilled Nafion and composite membranes were thus measured. Figure 7 shows a typical voltammetric curve resulting from electro-oxidation of methanol permeating the N_5SnO_2 membrane, J_{lim} value corresponding to the current densities plateau. The inset of Figure 7 shows J_{lim} values for N_RC, N_5SnO_2, and N_5S-SnO_2 membranes. Composites displayed lower J_{lim} than unfilled Nafion. The extent of the reduction of J_{lim} was 7%, and 50%, for N_5SnO_2, N_5S-SnO_2, respectively.

It is well-known that microstructure strongly influences the methanol transport properties of the electrolyte [8]. The possible occurrence of structural changes in the case of composites with respect to the unfilled Nafion membrane was investigated by XRD.

Figure 8 shows the XRD profiles of N_RC, N_5SnO_2, and N_5S-SnO_2 samples. In agreement with earlier reports [49-51], the recast Nafion membrane displayed a broad diffraction feature at 2θ = 12–22° which can be separated through deconvolution into two peaks, assigned to amorphous (2θ = 16°) and

For Peer Review

crystalline (2θ = 17.50 °) scattering from the polyfluorocarbon chains of Nafion. Crystallinity (X_{cr}) can be calculated from the ratio between the areas of the deconvoluted peaks. While crystallinity of recast Nafion was found to be 25%, in good agreement with the literature [50,51] the crystallinity of the composite membranes was higher, being 28% and 30% for N_5SnO$_2$, and N_5S-SnO$_2$ samples, respectively. This finding can be ascribed to a different crystalline structure or morphology induced by polymer/filler interactions. The increased crystallinity of composites obtained by incorporating different fillers in a Nafion membrane has already been reported [52, 53]. It is widely recognized that methanol crossover takes place both in the hydrophilic channel structure and in the hydrophobic backbone of the perfluorosulphonic ionomer [54, 55]. The increased crystallinity of the composites is indicative of a more compact hydrophobic region of the Nafion matrix which hinders the methanol infiltration thus explaining the reduced methanol crossover of composites with respect to the N_RC sample [56, 57].

The impedance characteristics of the DMFC under different operating temperatures (70-100 °C) were also investigated. All MEA components, except the membrane, were identical, therefore, the difference in the impedance spectra can be ascribed to the membrane and to the membrane/electrode interface. MEAs based on N_RC, N_5SnO$_2$, and N_5S-SnO$_2$ membranes were tested and the corresponding impedance spectra recorded at 90 °C, 100 °C and 110 °C are shown in Figure 9. All the spectra are characterized by the presence of two arcs, the high frequencies one accounting for the charge transfer and the low frequencies one accounting for mass transfer processes. The equivalent circuit, used to fit the spectra, is shown as an inset in Figure 9. R_{ele}, R_{ct}, and R_{mass} represent the ohmic resistance, charge transfer resistance and mass transfer resistance, respectively. R_{ct} accounts for both anode and cathode side, including methanol electro-oxidation and oxygen reduction reaction. On the other hand, since the cathode is fed with pure O_2, R_{mass} is dominated by methanol transport occurring at the anode side. L represents the inductive contributions and CPE is a constant phase element which replaces the conventional double-layer capacitance [58-61]. In the 70-110 °C range, R_{ele} was found to be weakly dependent on temperature for all samples; moreover, the differences in R_{ele} values of the three MEAs were not large enough to account for the different electrochemical performance showed in Figure 6. Therefore, such difference is mainly due to R_{ct} and R_{mass} which are related to the membrane/electrode interface.

Figure 10 shows the variation of R_{ct} (Figure 10a), and R_{mass} (Figure 10b), for the three MEAs as a function of temperature. At temperatures below 90 °C both resistances decreased for all samples. Above such temperature R_{ct} and R_{mass} show an abrupt increase for sample N_RC, while the values relative to the composites showed a steady decrease. The difference between unfilled Nafion and composites membranes is most evident at 100 °C and 110 °C, and highest in the case of N_5S-SnO$_2$, thus explaining the increased electrochemical performance shown in Figure 6 for such membrane.

The decrease of R_{ct} and R_{mass} observed for the composites is certainly related to the improved membrane/electrode interface stability associated with the superior dimensional stability induced by the presence of the fillers. To further enhance the quality of the electrolyte/electrodes interface the Nafion containing electrodes were brushed with a S-SnO$_2$/Nafion suspension to avoid the interfacial discontinuities and possible lack of adhesion expected when the unfilled Nafion membrane is replaced with the composite to assemble the MEA.

Figure 11 shows the resulting I-V and PD curves measured for the N_5S-SnO$_2$ sample at 100 °C and 110 °C. Comparing the data obtained with commercial electrodes at the two temperatures (Figure 6), it appears that the electrode modification lead to improved performance: in particular, a 32 % and a 22% increase in PD were observed at 100 °C and 110 °C, respectively. The best performance was observed at 110 °C, being PD_{max}= 100 mWcm^{-2} and $I_{(0.15V)}$ = 488 mAcm^{-2}.

In-situ EIS spectra of the N_5S-SnO$_2$ cell equipped with modified electrodes were also acquired. Figure 12 shows the impedance spectra recorded at 90 °C,100 °C and 110 °C, the inset showing R_{ct} and R_{mass} as a function of temperature in the 70-110 °C range. Both R_{ct} and R_{mass} decrease as the temperature increased; R_{mass} values were similar to that recorded for the unbrushed MEA, while R_{ct} values were appreciably lower indicating that the brushing technique is a successful method to enhance the electrode/electrolyte interface.

Combining the brushing technique with the use of N_5S-SnO$_2$ composite membrane as electrolyte allowed to enable the Nafion membrane to endure higher temperatures, achieving at 110 °C a power density improvement of 52% with respect to the unfilled Nafion membrane.

4 Conclusions

The introduction of proton conducting fillers such as hydrated tin oxide ($SnO_2 \cdot nH_2O$) and its sulfated derivative (S-SnO_2) have a positive effect of on the properties of Nafion membranes. The higher degree of crystallinity of the composites with respect to a polymer unfilled membrane indicated by XRD measurements demonstrate that such structural modification results in reduced methanol crossover (up to 50 %) as derived from J_{lim} measurements. The additional acidic sites provided by the superacidic inorganic compound where bidentate sulfate groups are coordinated to the oxide particles (S-SnO_2) also improved the proton transport characteristics of the Nafion membrane.

When assembled in a MEA, such composite electrolytes display an enhanced membrane/electrode interface stability as revealed by electrochemical impedance spectroscopy. The adhesion and chemical continuity of such interface can be further improved by incorporating the sulfated filler on the electrodes. MEAs fabricated with modified electrodes and composite Nafion membrane containing 5 wt% S-SnO_2 allowed to operate a DMFC at 110 °C obtaining PD_{max}=100 $mWcm^{-2}$, and $I_{(0.15V)}$= 488 $mAcm^{-2}$, *i.e.* a 52% power density improvement with respect to the unfilled Nafion membrane.

Acknowledgments

The financial support of the Ministry for Foreign Affairs (Italy-Quebec Joint Lab for Advanced Nanostructured Materials for Energy, Catalysis and Biomedical Applications) is gratefully acknowledged.

Thanks are due to Prof. Ana Tavares (INRS-EMT, Varennes, Québec, CANADA) for help in collecting and discussing FT-IR spectra.

References

[1] S. Wasmus, A. Küver, *J. Electroanal. Chem.* **1999**, *461*, 14.
[2] X. Ren, P. Zelenay, S. Thomas, J. Davey and S. Gottesfeld, *J. Power Sources* **2000**, 86, 111.
[3] N.W. De Luca, Y.A. Elabd, *J. Polymer Sci. Part B: Polymer Physics* **2006**, *44*, 2201.
[4] V. Neburchilov, J. Martin, H. Wang, J. Zhang, *J. Power Sources* **2007**, *169*, 221.
[5] S. J. Paddison and R. Paul, *Phys. Chem. Chem. Phys.* **2002**, *4*, 1158.
[6] K.A. Mauritz, R.B. Moore, *Chem. Rev.* **2004**, *104*, 4535.
[7] D. E. Moilanen, D. B. Spry, and M. D. Fayer, *Langmuir* **2008**, *24,* 3690.
[8] K.D. Kreuer, *J. Membrane Sci.* **2001**, *185*, 29.
[9] M. Casciola, G. Alberti, M. Sganappa, R. Narducci, *J. Power Sources* **2006**, *162*, 141.
[10] C.H. Lee, S.Y. Lee, Y.M. Lee, S.Y. Lee, J.W. Rhim, O. Lane, and J.E. McGrath, *ACS Appl. Mater. Interfaces* **2009**, *1*, 1113.
[11] G. Alberti M. Casciola, *Annu. Rev. Mater. Res.* **2003**, *33*,129;
[12] D. Jones, J. Roziere, *Adv. Polym. Sci.* **2008**, *215*, 219
[13] P.L. Antonucci, A.S. Aricò, P. Cretì, E. Ramunni, V. Antonucci, *Solid State Ionics* **1991**, *25*, 431
[14]N. Miyake, J.S. Wainright and R.F. Savinell, *J. Electrochem. Soc.* **2001**, *148*, A905
[15] V. Baglio, A.S. Aricò, A. Di Blasi, V. Antonucci, P.L. Antonucci, S. Licoccia, E. Traversa, F. Serraino Fiory, *Electrochimica Acta* **2005**, *50*, 1241.
[16] N.H. Jalani, K.Dunn, R.Datta, *Electrochimica Acta* **2005**, *51*, 553.
[17] D.H. Jung, S.Y. Cho, D.H. Peck, D.R. Shin and J.S. Kim, *J. Power Sources* **2002**, *106*, 173.
[18] G. Alberti, M. Casciola, D. Capitani, A. Donnadio, R. Narducci, M. Pica, M. Sganappa, *Electrochimica Acta* **2007**, *52*, 8125.
[19] P. Costamagna, C. Yang, A.B. Bocarsly, S. Srinivasan, *Electrochim. Acta* **2002**, *47*,1023.
[20] M.Casciola, D.Capitani, A.Comite, A.Donaddio, V.Frittella, M.Pica, M.Sganappa, and A.Varzi, *Fuel Cells* **2008**, *3-4*, 217.
[21] S. Malhotra, R. Datta, *J. Electrochem. Soc.* **1997**, *144*, L23.
[22] T.M. Thampan, N.H. Jalani, P. Choi, R. Datta, *J. Electrochem. Soc.* **2005**, *152*, A316.
[23] M.A.Navarra, F.Croce, and B.Scrosati, *J. Mater. Chemistry* **2007**, *17*, 3210.
[24] M.A. Navarra, C.Abbate, B.Scrosati, *J. Power Sources* **2008**, *183*, 109.
[25] A. D'Epifanio, M. A. Navarra, F. C. Weise, B. Mecheri, J. Farrington, S. Licoccia and S. Greenbaum, *Chem. Mater*., DOI:10.1021/cm901486t.
[26] A.S.Aricò, V.Baglio, A. Di Blasi, P.Creti, P.L. Antonucci, V.Antonucci, *Solid State Ionics* **2003**,161, 251.
[27] B.Mecheri, A.D'Epifanio, E.Traversa and S.Licoccia, *J. Power Sources* **2008**, *178*, 554.
[28] B.Mecheri, A. D'Epifanio, L. Pisani, F. Chen, E. Traversa, F. C.Weise, S. Greenbaum, and S. Licoccia, *Fuel Cells* **2009**, *4*, 372.

For Peer Review

[29] H. Matsuhashi, H. Miyazaki, Y. Kawamura, H. Nakamura, and K. Arata, *Chem. Mater.* **2001,** *13,* 3038.
[30] A.S. Khder, A.I. Ahmed, Applied Catalysis A: General **2009,** 354, 153–160.
[31] S Furuta, H Matsuhashi, K Arata, *Catal. Commun.* **2004**, *5*, 721.
[32] S Furuta, H Matsuhashi, K Arata , *Applied Catalysis A: General*, **2004**, 257, 213.
[33] N.Spanos, I.Georgiadou, and A.Lycourghiotis, J.Coll.Int.Sci. **1995**, 172, 374.
[34]A. D'Epifanio, B. Mecheri, E. Fabbri, A.Rainer, E. Traversa and S. Licoccia J. Electrochem. Soc., **2007,** 154, B1148.
[35] A. Gamard, O. Babot, B. Jousseaume, M.-C. Rascle, T. Toupance, and G. Campet, *Chem. Mater.* **2000,** *12,* 3419-3426.
[36] J.Zhang and L.Gao, J. Solid State Chem. **2004**, 177, 1425.
[37] H. Matsuhashi, M. Hino, K. Arata, Appl. Catal. **1990**, A59, 205.
[38] S. Furuta, H. Matsuhashi,K. Arata *Applied Catalysis A:* **2004,** 269, 187–191.
[39] M.A. Martin, J.W. Childers, and R.A. Palmer, Appl. Spectrosc., **1987,** 41,120.
[40] H. Tamura, A. Tanaka, K. Mita, and R. Furuichi, Journal of Colloid and Interface Science **1999,** 209**,** 225–231.
[41] W.A. England, M.G. Cross, A.Hammett, P.J. Wiseman and J.B. Goodenough*, Solid State Ionics,* **1980***, 1,* 231
[42] A.S. Khder, E.A. El-Sharkawy, S.A. El-Hakam , A.I. Ahmed, Catalysis Communications **2008,** 9, 769–777.
[43] S. Hara, H. Sakamoto, M. Miyayama and T. Kudo, *Solid State Ionics* **2002**, *154–155,* 679.
[44] S. Hara, S. Takano and M. Miyayama, *J. Phys. Chem. B* **2004**, *108*, 634.
[45] E.W. Giesekke, H.S. Gutowsky, P. Kirkov and H.A. Laitenen, *Inorg. Chem.* **1967**, *6*, 1294
[46] R. Gutiérrez-Báez, J. A. Toledo-Antonio, M. A. Cortes-Jácome, P. J. Sebastian, and A. Vázquez, *Langmuir* **2004**, *20*, 4265.
[47] H.Matsuhashi, M. Hino, K.Arata, Chem. Lett. **1988**, 1027.
[48] Vladimir Neburchilov, Jonathan Martin, Haijiang Wang , Jiujun Zhang, Journal of Power Sources **2007,**169, 221–238.
[49] R.B. Moore III, C.R. Martin, *Macromolecules* **1988**, *21*, 1334.
[50] T.D. Gierke, G.E. Munn, F.C. Wilson, *J. Polym. Sci. Phys.* **1981**, 19, 1687.
[51] M. Fujimura, T. Hashimoto, and H. Kawai, *Macromolecules* **1981,** *14,* 1309.
[52] F. Bauer, M. Willert-Porada, J. Membrane Sci. **2004**, *233*, 141.
[53] Z. Wu, G. Sun, W. Jin, H. Hou, S. Wang, Q. Xin, *J. Membrane Sci.* **2008**, *313*, 336.
[54] P. Dimitrova, K.A. Friedrich, U. Stimming , B. Vogt, *Solid State Ionics* **2002**, *150*, 115.
[55] A. Heinzel, V.M. Barragan, *J. Power Sources* **1999**, *84*, 70.
[56] P. Dimitrova, K.A. Friedrich , B. Vogt, U. Stimming *J. Electroanal. Chem.* **2002**, *532*, 75.
[57] Y.S. Park, Y. Yamazaki, *Solid State Ionics* **2005**, *176*, 1079.
[58] Mueller, J. T.; Urban, P. M. *J. Power Sources* **1998**, *75*, 139.
[59] P. Piela, R. Fields and P. Zelenay, *J. Electrochem. Soc.* **2006**,*153*, A1902.
[60] X.Yuan, H.Wang, J.C. Sun, J. Zhang, *Int. J. Hydrogen Energy* **2007**, *32*, 4365.
[61] S.Seo and C.S. Lee, *Energy & Fuels* **2008**, *22*, 1204.

For Peer Review

Figure Captions

Fig. 1 XRD patterns of $SnO_2 \cdot nH_2O$ and S-SnO_2 powders.
Fig. 2 EDX spectrum of $SnO_2 \cdot nH_2O$ and S-SnO_2
Fig. 3 FT-IR spectra of $SnO_2 \cdot nH_2O$ and S-SnO_2
Fig. 4 TG profiles of $SnO_2 \cdot nH_2O$ and S-SnO_2 powders.
Fig. 5 Proton conductivity values of unfilled Nafion and composite membranes at 100°C and 110°C (RH=100%).
Fig. 6 Polarization and power density curves of unfilled Nafion and composite membranes at (a) T=100°C and (b) T=110°C. Anode feed: 2M aqueous methanol, flow rate 2.5 $mLmin^{-1}$, pressure 2 abs bar. Cathode feed: O_2 flow rate 100 sccm, pressure 2 abs bar
Fig. 7 Voltammetric curve for the oxidation of methanol permeating through the N_5SnO_2 membrane exposed to a 2M methanol feed. T=80°C. Inset: Limiting current density (J_{lim}) values of N_RC, N_5SnO_2, and N_5S-SnO_2 membranes.
Fig. 8 XRD patterns of N_RC, N_5SnO_2, and N_5S-SnO_2 membranes.
Fig. 9 Impedance spectra of MEAs made up with N_RC, N_5SnO_2 and N_5S-SnO_2 membranes as electrolytes, during DMFC functioning at 90°C, 100°C and 110°C. Anode feed: 2M aqueous methanol. Cathode feed: O_2.
Fig. 10 Charge transfer resistance, R_{ct} (a) and mass transfer resistance, R_{mass} (b) as a function of temperature for MEAs made up with N_RC, N_5SnO_2 and N_5S-SnO_2 membranes as electrolytes.
Fig. 11 Polarization and power density curves of the MEA prepared by brushing and containing N_5S-SnO_2 membrane as electrolyte at (a) T=100°C and (b) T=110°C. Anode feed: 2M aqueous methanol, flow rate 2.5 $mLmin^{-1}$, pressure 2 abs bar. Cathode feed: O_2 flow rate 100 sccm, pressure 2 abs bar.
Fig.12 Impedance spectra of the MEA prepared by brushing and containing N_5S-SnO_2 membrane as electrolyte, during DMFC functioning at 90°C, 100°C and 110°C. Anode feed: 2M aqueous methanol. Cathode feed: O_2. Inset: Charge transfer resistance, R_{ct} (a) and mass transfer resistance, R_{mass} (b) as a function of temperature.

For Peer Review

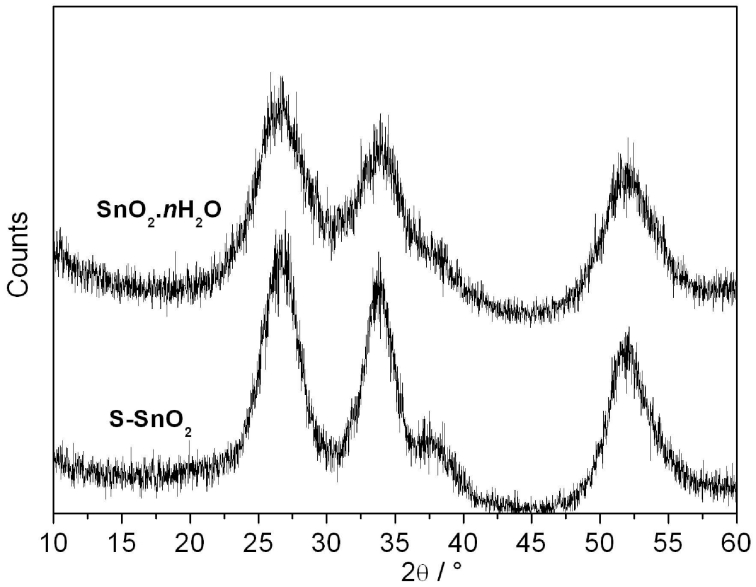

Fig. 1 XRD patterns of SnO_2•nH2O and S-SnO2 powders.
297x209mm (200 x 200 DPI)

Review

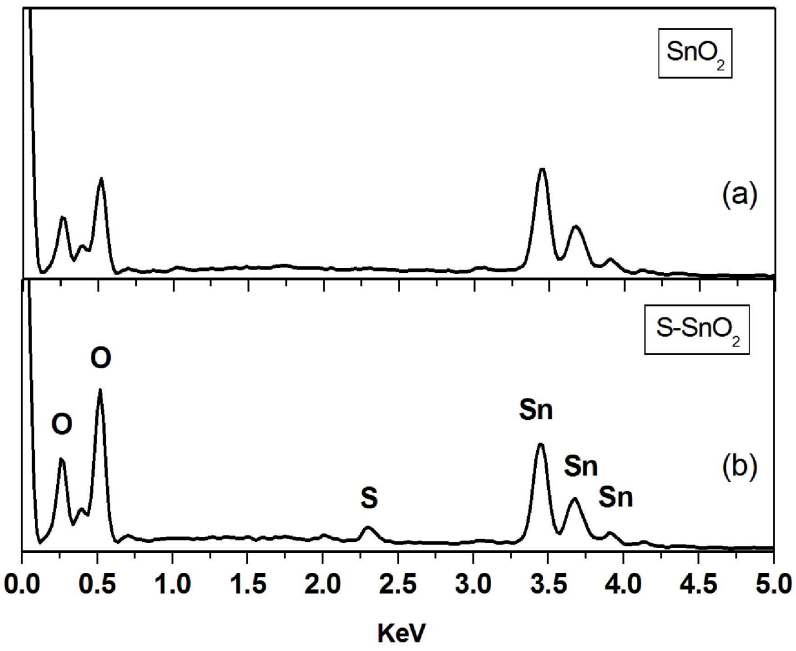

279x215mm (200 x 200 DPI)

Review

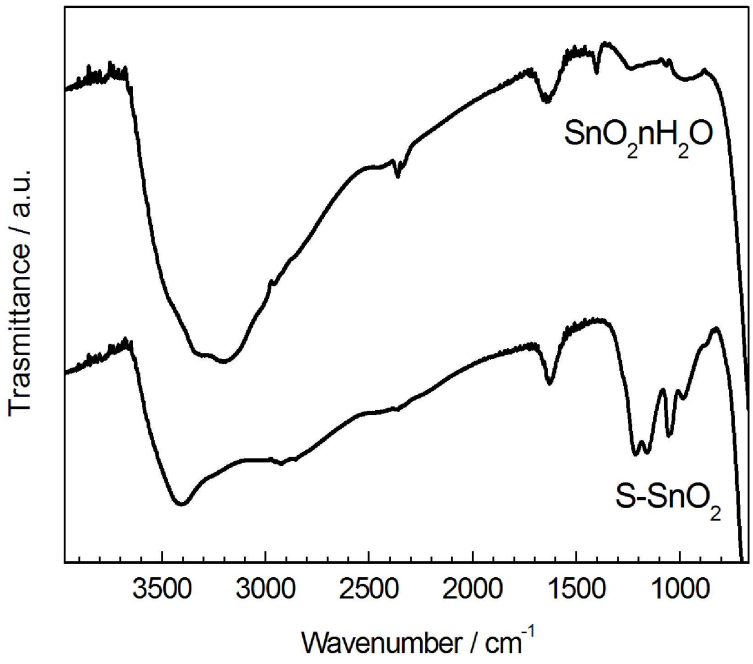

Fig. 3 FT-IR spectra of SnO2•nH2O and S-SnO2
279x215mm (200 x 200 DPI)

Review

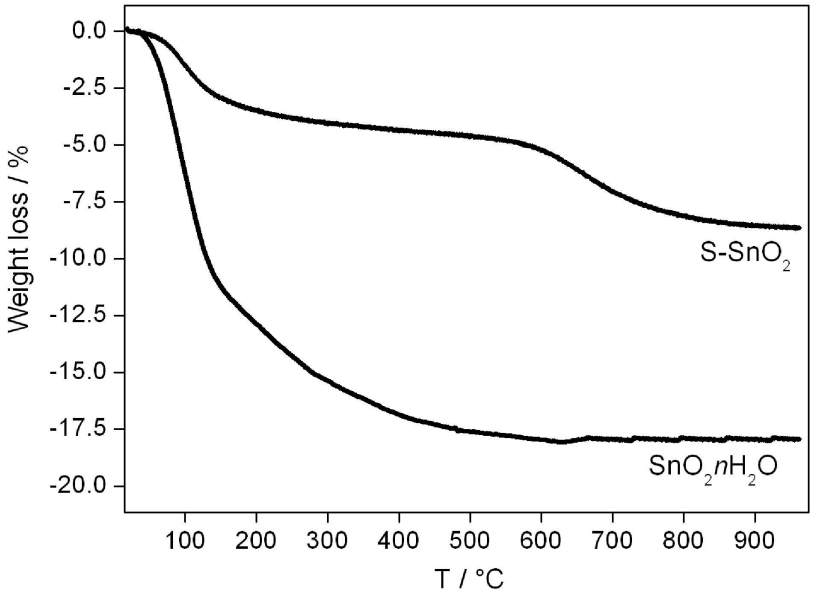

Fig. 4 TG profiles of SnO2•nH2O and S-SnO2 powders.
Fig. 5 Proton conductivity values of unfilled Nafion and composite membranes at 100°C and 110°C (RH=100%).

297x209mm (200 x 200 DPI)

Review

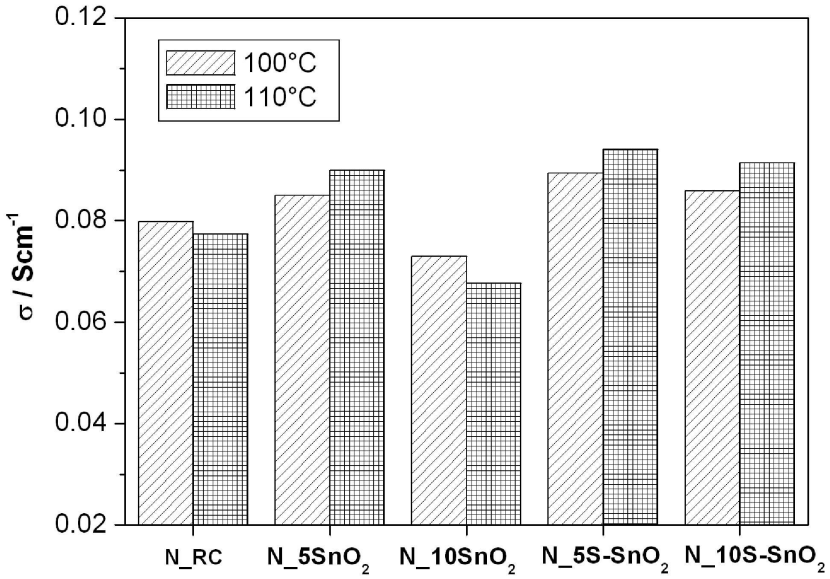

Fig. 5 Proton conductivity values of unfilled Nafion and composite membranes at 100°C and 110°C (RH=100%).
297x209mm (200 x 200 DPI)

Review

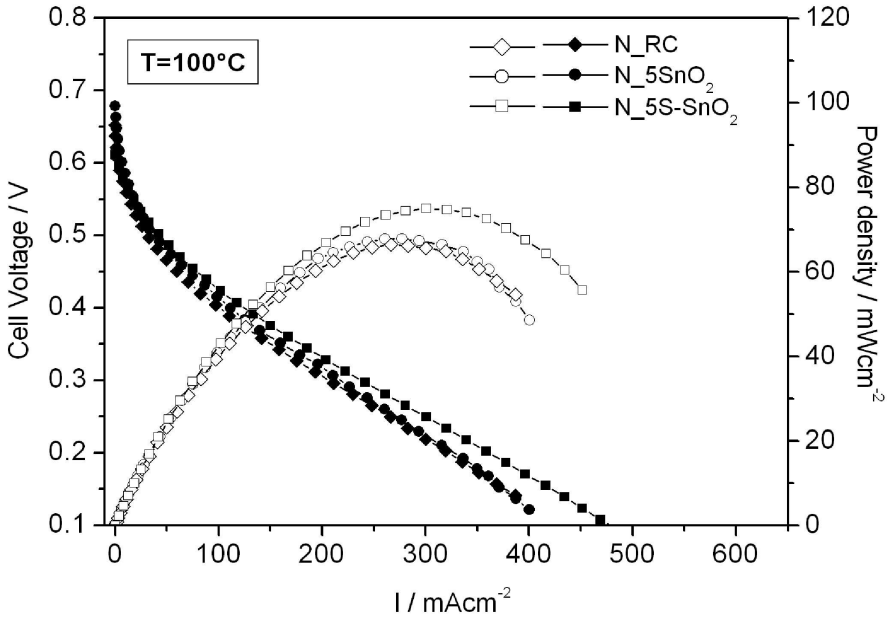

Fig. 6b Polarization and power density curves of unfilled Nafion and composite membranes at (a) T=100°C and (b) T=110°C. Anode feed: 2M aqueous methanol, flow rate 2.5 mLmin-1, pressure 2 abs bar. Cathode feed: O2 flow rate 100 sccm, pressure 2 abs bar.
297x209mm (200 x 200 DPI)

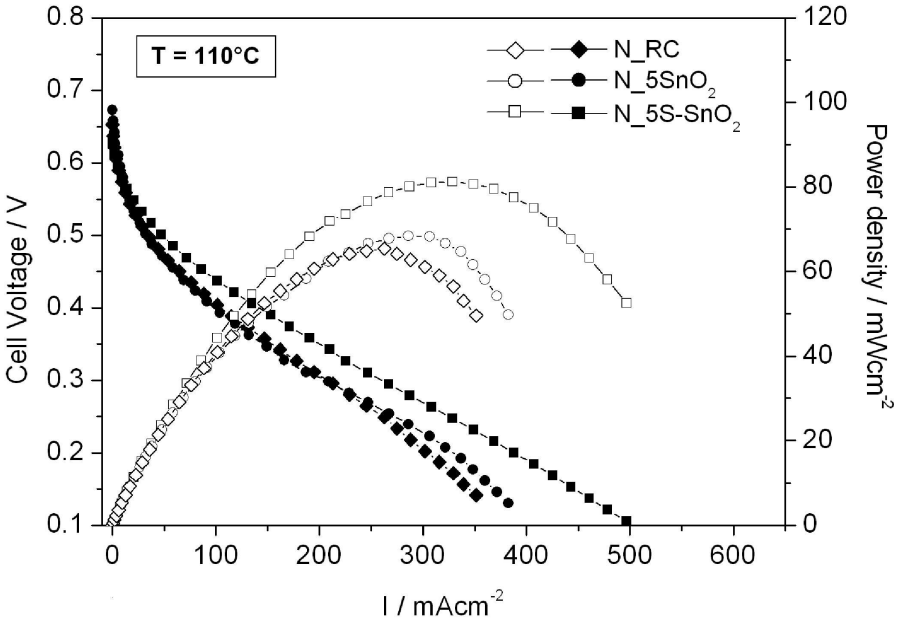

Fig. 6 Polarization and power density curves of unfilled Nafion and composite membranes at (a) T=100°C and (b) T=110°C. Anode feed: 2M aqueous methanol, flow rate 2.5 mLmin-1, pressure 2 abs bar. Cathode feed: O2 flow rate 100 sccm, pressure 2 abs bar.
297x209mm (200 x 200 DPI)

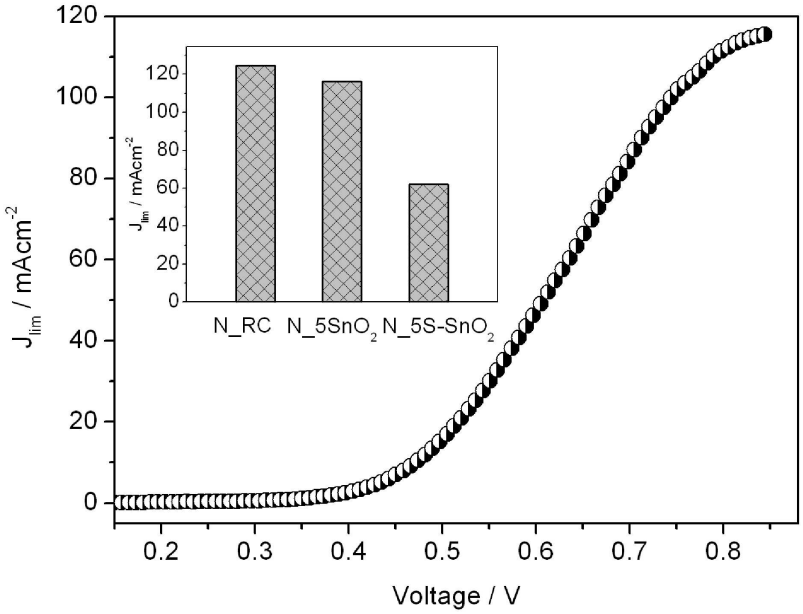

Fig. 7 Voltammetric curve for the oxidation of methanol permeating through the N_5SnO2 membrane exposed to a 2M methanol feed. T=80°C. Inset: Limiting current density (Jlim) values of N_RC, N_5SnO2, and N_5S-SnO2 membranes
297x209mm (200 x 200 DPI)

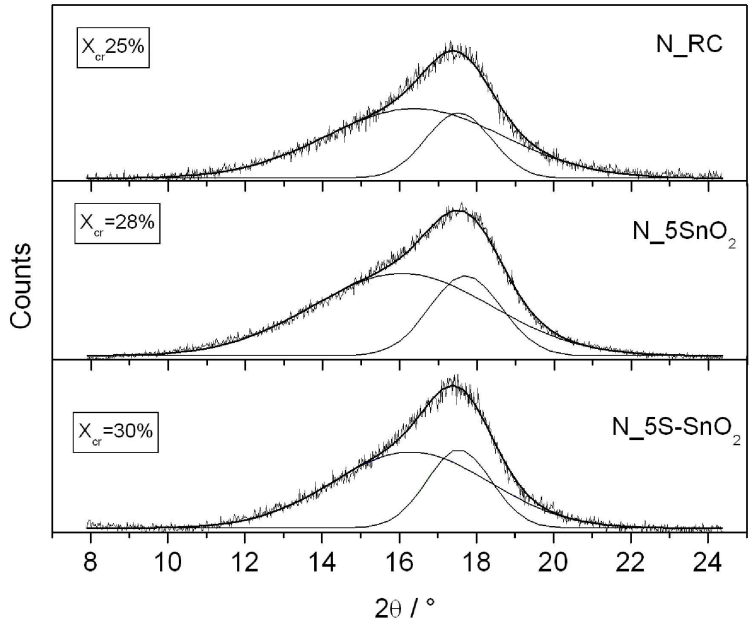

Fig. 8 XRD patterns of N_RC, N_5SnO2, and N_5S-SnO2 membranes.
297x209mm (200 x 200 DPI)

Review

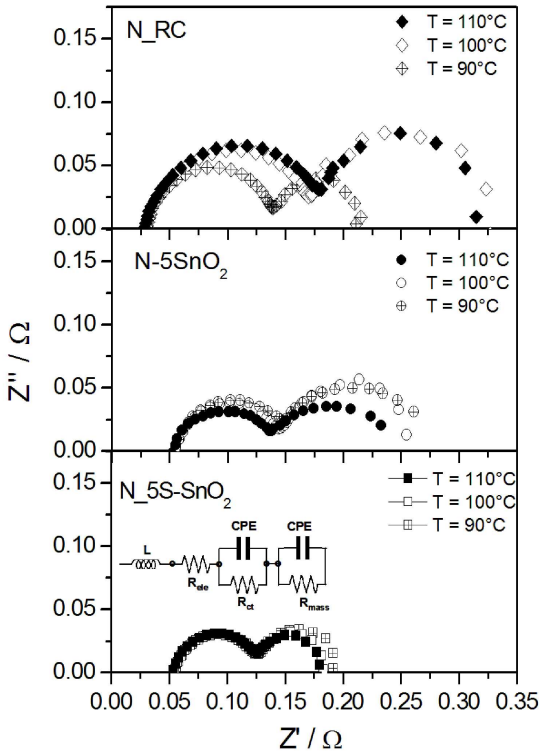

Fig. 9 Impedance spectra of MEAs made up with N_RC, N_5SnO2 and N_5S-SnO2 membranes as electrolytes, during DMFC functioning at 90°C, 100°C and 110°C. Anode feed: 2M aqueous methanol. Cathode feed: O2.
279x215mm (250 x 250 DPI)

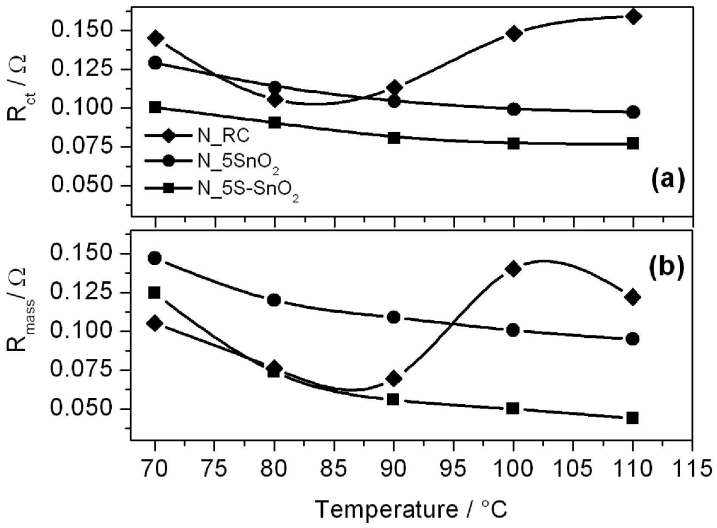

Fig. 10 Charge transfer resistance, Rct (a) and mass transfer resistance, Rmass (b) as a function of temperature for MEAs made up with N_RC, N_5SnO2 and N_5S-SnO2 membranes as electrolytes. 297x209mm (200 x 200 DPI)

Review

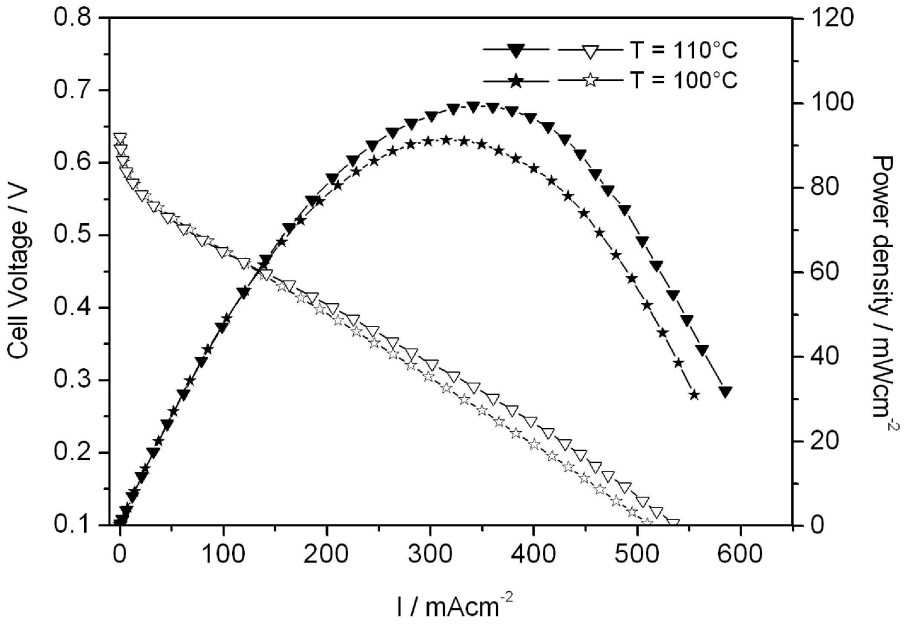

Fig. 11 Polarization and power density curves of the MEA prepared by brushing and containing N_5S-SnO2 membrane as electrolyte at (a) T=100°C and (b) T=110°C. Anode feed: 2M aqueous methanol, flow rate 2.5 mLmin-1, pressure 2 abs bar. Cathode feed: O2 flow rate 100 sccm, pressure 2 abs bar.
297x209mm (200 x 200 DPI)

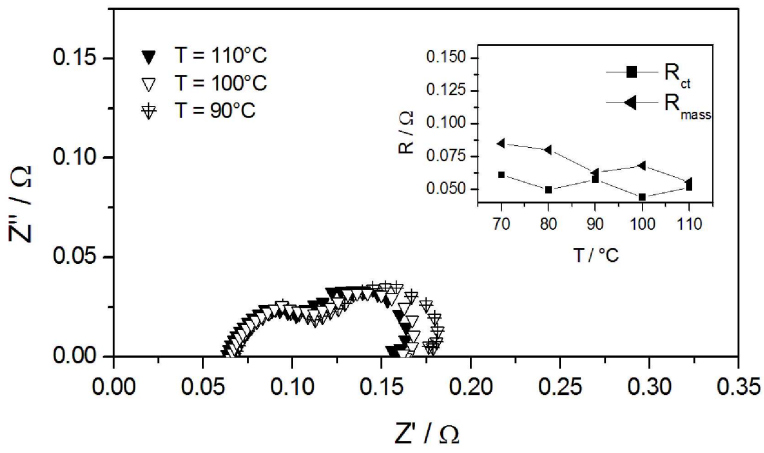

Fig.12 Impedance spectra of the MEA prepared by brushing and containing N_5S-SnO2 membrane as electrolyte, during DMFC functioning at 90°C, 100°C and 110°C. Anode feed: 2M aqueous methanol. Cathode feed: O2. Inset: Charge transfer resistance, Rct (a) and mass transfer resistance, Rmass (b) as a function of temperature.
279x215mm (200 x 200 DPI)